


**Multiple constraints on nuclear mass formulas for reliable extrapolations**

Wei-hu Ye and Yi-bin Qian\*

*Department of Applied Physics, Nanjing University of Science and Technology, Nanjing 210094, China  
and MIT Key Laboratory of Semiconductor Microstructure and Quantum Sensing,  
Nanjing University of Science and Technology, Nanjing 210094, China*Hankui Wang<sup>†</sup>*Department of Physics, Zhejiang SCI-TECH University, Hangzhou 310018, China  
and Key Laboratory of Optical Field Manipulation of Zhejiang Province, Zhejiang SCI-TECH University, Hangzhou 310018, China* (Received 6 October 2022; revised 17 February 2023; accepted 24 March 2023; published 5 April 2023)

Nuclear mass is responsible for many key processes in both nuclear physics and astrophysics. While the theoretical accuracy of masses has reached a quite astonishing level, the extrapolations among various predictions have been conflicting due to several possible reasons, such as the missing physics and overfitting problems in current formulas. Instead of the single target of binding energies, we make use of both the  $\alpha$  decay energy and the Garvey-Kelson relations as multiple physical constraints on mass models to address the above issues to some extent. By means of the multiobjective optimization, the Bethe-Weizsäcker-type and the Duflo-Zucker (DZ) mass models are carried out to perform such a study as specific examples. Thanks to very recent measured neutron-rich nuclei beyond the AME20, we further test the predictive power on two DZ-type formulas as accompanied by the impressive accuracy. The discrepancies between the predicted values of the DZ10 and the DZ33 can be significantly reduced, which implies the therapy of the overfitting phenomenon in some degree. This leads to lower uncertainties of extrapolations for the models themselves.

DOI: [10.1103/PhysRevC.107.044302](https://doi.org/10.1103/PhysRevC.107.044302)**I. INTRODUCTION**

Nuclear mass or binding energy (BE) is an essential property of nuclei. It plays a paramount role in understanding rich nuclear structure information such as nuclear effective interactions, stability, reaction rates, and so on [1]. Meanwhile, it is one of the most important nuclear physics inputs that can greatly affect the  $r$  process of nucleosynthesis in astrophysics, which is quite important to answer a question: How are elements heavier than iron made in nature [2–4]? As a result, a precise knowledge of nuclear masses is urgently required for many branches of nuclear science. Experimental explorations have been very successful in measuring around 2500 masses with the high precision via the direct or indirect methods. A range for the total number of bound nuclei between 7000 to 10000 is typical for a wide variety of state-of-the-art nuclear theories [4,5]. Note that thousands of exotic nuclei involving the  $r$  process is unreachable experimentally in the foreseeable future, the theoretical investigations are becoming increasingly important aiming at providing the reliable extrapolations.

Both macroscopic-microscopic and purely microscopic considerations have been developed to reproduce available data, yielding the root mean square deviations (RMSD) between predicted and measured values in the range of 300–5000 keV [6]. Besides, there are a series of local mass

formulas from the unique relations of neighboring nuclei, particularly the famous Garvey-Kelson relations (GKs) [7]. In recent years, machine learning has been demonstrated to be a promising tool for learning the missing physics and improving the accuracy to a higher level towards the precision of a hundred keV [8–14]. This indicates that the masses predicted by the machine learning approach have satisfied the accuracy requirement for astrophysics applications in known regions.

When it comes to extrapolations, it is expected that a theoretical model that describes known masses well also has the ability to accurately predict the rest of the nuclear landscape, but recently this assumption has been critically examined and proved to be doubtful [15–17]. This implies that the predictive power of models may not fully depend on the theoretical accuracy of masses in the known region since so many factors are involved in the extrapolation. Also, the mass differences between various models tend to grow with the increase of the extrapolation distance [18–20]. Although the models are equipped with the Bayesian neural network or the radial basis function, their prediction differences are still large [11]. The reasons may come from two directions. One is the missing physics that is not yet to be incorporated into mass formulas. For instance, the shell evolution has been observed in the experimental side [21–23]. Considering that most of the global models usually correspond to the specific shell structure, some adjustments on magic number may be required in calculating those nuclei with extreme isospin asymmetry for mass models. On the other hand, such parametrization models are born with two drawbacks, namely, underfitting

\*qyibin@njust.edu.cn

†whk2007@163.com

and overfitting problems [24]. The latter one is relevant with this paper, which can be understood as one source of the statistical uncertainties. Assuming that overfitted models, being flawless in the physical perspective, can perfectly reproduce the samples in the fitting set, but they cannot correctly predict the samples far away from training samples because of the lack of constraints of enough data, causing the parameters of models determined by fitting the experimental data to be prone to being locally optimal rather than globally optimal. Simply stated, the underlying physics in models may be additionally attached into the parameter of models for singly pursuing the so-called mass optimal solution, which is reflected in the fact that the “byproducts” (nucleon separation energy, decay energy) extracted from the mass models show the uncontrollable deviations to be much larger or smaller than the accuracy of binding energies and the more troublesome is the nontrivial disagreement among various models [20]. More physical constraints, hence, should be introduced into fitting procedure to reduce the risk of overfitting and in so doing better guiding the extrapolation.

One potential way to tackle the above dilemmas is to employ the multiobjective optimization (MOO) by including more physical constraints on mass formulas, which is an effective way to heal the overfitting problem for providing more training samples in fitting procedures [24]. The MOO is devoted to optimize more than one objective problem and the relationship among objectives are generally conflicting and repulsive [25,26]. Recently, we initially performed the MOO strategies on mass models by including the  $\alpha$  decay energies [27], while the key issues, such as further reducing the model uncertainty and extrapolation differences between models, remain missing. In the present work, we carry out a more thorough and rigorous method to narrow the range of solutions that may achieve more reliable predictions. The extrapolation differences between DZ10 and DZ33 are evaluated in a reasonable way, suggesting that the MOO strategies can somewhat reduce the prediction differences between models. Furthermore, the GKs, as discussed above, are a very crucial condition since they indicate the local features of neighboring nuclei and the cancellation of the isospin dependence of the residual interaction. The GK mass relations are, therefore, introduced as a physical constraint on mass models, and also a test to check the compatibility between GKs and mass models. This paper is structured as follows. In Sec. II, we briefly make an introduction for the MOO and the mass models including the Bethe-Weizsäcker 2 (BW2), the DZ10, the DZ33, and the GK mass formulas. In Sec. III, the improved accuracy of observables is discussed. The method to select potential solutions for the extrapolations at long distance is presented, and further the comprehensive performance as well as extrapolation uncertainties of models are evaluated and analyzed in detail. The summary is drawn in the last section.

## II. DESCRIPTION OF THE MOO AND THE MASS MODELS

### A. Multiobjective optimization

Real-life systems usually require the simultaneous optimization of multiple and related objectives, while a solution

is usually optimal for one objective but not the cases for other objectives. Within this situation, the concept of MOO naturally arises. The MOO defines Pareto optimal or Pareto front (PF) set, a set of solutions, in which the rank of each solution is equal in contrast to one best solution in the single objective evolution algorithms (SOEAs). A multiobjective problem can be described as

$$\begin{aligned} \min \quad & F(x) = (f_1(x), \dots, f_m(x)), \\ & \text{lb} \leq x_i \leq \text{ub}, \end{aligned} \quad (1)$$

where  $f_{1-m}(x)$  is the related objective functions, and  $x = (x_1, x_2, \dots, x_m)$  is the decision variables in which  $x_i$  is restricted in lower bound and upper bound. The Pareto dominance is defined as: a solution  $j$  is dominated by another feasible solution  $k$  if  $f_i(j) \geq f_i(k)$  for  $i = 1, 2, \dots, m$  and  $f_i(j) > f_i(k)$  for at least one objective function. This important definition leads to the content and detail of MOO. There has been much progress in developing universal multiobjective evolution algorithms (MOEAs) for locating the ideal Pareto front for the decades, including but not limited to covariance matrix adaptation evolution strategy [28], strength Pareto evolutionary algorithm 2 [29], Pareto archived evolution strategy [30]. Of course, one can assign a weight factor ( $\omega_i > 0$ ,  $\sum_i^m \omega_i = 1$ ) to individual objectives and combine them together as a composite function ( $\sum_{i=1}^m f_i \omega_i$ ) to be optimized using any SOEAs. The priority of objectives according to the preference of users can be determined via the weight factors, but in practice it is very difficult to determine the weight factors even for those who are familiar with this method [25]. Thus, for more complicated problems with many functions and decision variables one has to rely on specific multiobjective algorithms. The nondominated sorting genetic algorithm-III (NSGA-III) [31] is employed here. The detailed discussions on algorithm are given below.

The basic philosophy of evolutionary algorithms is inspired in biological evolution. All individuals in a population including parent and offspring compete simultaneously with one another. The individuals with larger adaptive capacity survive and these surviving elites as a new parent generate the next generation. The above procedures continually run in ideal environment. The best individuals thus will be obtained from the end of loop.

The simplified steps for the NSGA-III are shown in Fig. 1. It would be easier to understand if one combines Fig. 1 and the following discussion on NSGA-III. At the  $t$ th generation, a parent population  $P_t$  having  $N$  members is randomly generated, where  $t$  denotes the number of generations, and the offspring  $Q_t$  with the same number  $N$  is created via performing mutations, simulated binary crossover operator, and selections on the  $P_t$ . These two populations are combined together to create a new population  $R_t = P_t \cup Q_t$  with size  $2N$ . In order to find excellent individuals from  $R_t$  efficiently for the next generation, the fast nondominated sorting and the reference point procedure will be performed, which are the essence of NSGA-III. The NSGA-III inherits the fast nondominated sorting proposed in NSGA-II [32]. The fast nondominated sorting procedure is used to divide the population into different nondominated level ( $F_1, F_2, \dots, F_i$ ), starting from  $F_1$ ,

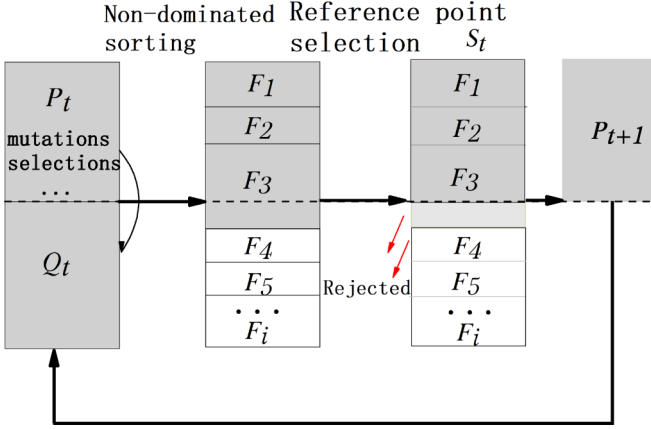


FIG. 1. Basic steps of the NSGA-III illustrated by this sketch. By using the nondominated sorting procedure, all individuals are assigned to different class in order of their convergence, starting from  $F_1$ , and the individual belonging to  $F_1$  is more convergent than the individual in  $F_2$ . The reference point procedure is used to precisely select the solutions that will maximize the diversity of the last chosen front. These steps shown in Fig. 1 run and iterate until the number of iterations is reached or the results are convergent.

where  $F_1$  denotes the first nondominating front. Next, all solutions of each nondominated front are successively added into a new population  $S_t$  in order of front. If the  $S_t$  fits the size of the population completely, it will be regarded as the next parent, namely,  $S_t = P_{t+1}$ . No further operations are needed. However, once the  $S_t$  exceeds  $N$  for the first time after adding a set of nondominating fronts, the reference point procedure will be performed to reject partial solutions from the last chosen nondominating front and all the remaining fronts for matching the number of  $N$ . In Fig. 1 after adding the front of  $F_3$ , the  $S_t$  exceeds  $N$  for the first time. Then, the reference point procedure is started and the remaining fronts ( $F_4, F_5, \dots, F_i$ ) will be immediately removed from the  $S_t$ . The rejected solutions are less diverse than the other solutions in this front. The reference points are a set of predefined points on a normalized hyperplane to structure the search space. The calculation of reference points is described as  $H = \frac{(M+p-1)!}{p!(M-1)!}$ , where  $H$  and  $M$  represent the number of reference points and objectives, respectively, and  $p$  denotes the amount of subdivisions along each objective, which can be set by the user. An example is shown in Fig. 2 with  $M = 3$ ,  $p = 4$ . One can see from Fig. 2 that the 15 reference points are well distributed on the entire normalized hyperplane, the obtained solutions are also likely to be widely distributed on this plane. (See Refs. [31,33,34] for more detail.)

## B. Mass models

It is necessary to provide some proper descriptions for the mass models employed and the corresponding GKs. The BW2 is an improved version of the classical liquid drop model with more physical terms considered. The BW2 employed in this

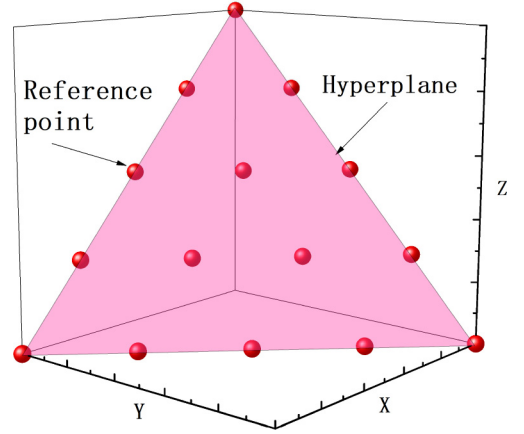


FIG. 2. A sketch of the reference points on a hyperplane for a three objectives problem.

work is taken from Ref. [35] and can be modified as

$$\begin{aligned}
 BE_{BW2} = & a_1A - a_2A^{2/3} - a_3Z^2A^{-1/3} + a_4\frac{Z^{4/3}}{A^{1/3}} \\
 & - a_5\frac{(N-Z)^2}{A} + a_6\frac{(N-Z)^2}{A^{4/3}} - a_7\frac{|N-Z|}{A} \\
 & + a_8\delta A^{-1/2} + a_9A^{1/3} - a_{10}P + a_{11}P^2, \quad (2)
 \end{aligned}$$

where  $a_i$  are the free parameters determined by fitting experimental nuclear masses. The  $\delta = [(-1)^N + (-1)^Z]/2$  and  $P = v_p v_n / (v_n + v_p)$  are associated with pairing and shell correction terms, where  $v_p$  ( $v_n$ ) denotes the difference between the nearest magic numbers and proton (neutron) numbers.

The DZ family have amply shown their niche in the mass model market not only with the good agreement between experimental and predicted values (about 350–550 keV) but also with the reliability and validity in terms of an extrapolation issue [36,37]. Meanwhile, they have been applied in astrophysical investigations, such as the properties of neutron stars [17], and the extraction of symmetry energy to predict the neutron skin thickness [27,38]. The popularity of the DZ family in some sense can be attributed to its relatively low computational cost since every term of which is an algebraic analytical expression, allowing us to make statistical strategies on it with less cost by using Monte Carlo methods [39].

The simpler DZ10 contains ten terms which can be classified into two groups. The six microscopic terms are built from the interacting shell model. The remaining four macroscopic terms considering global behavior of nuclei are the Coulomb  $V_C$ , symmetry energy  $V_T$  and its surface corrections  $V_{TS}$ , and pairing energies  $V_P$ . The DZ10 mass formula can be written as

$$\begin{aligned}
 BE_{DZ10} = & a_1V_C + a_2(M+S) - a_3\frac{M}{\rho} - a_4V_T \\
 & + a_5V_{TS} + a_6s_3 - a_7\frac{s_3}{\rho} + a_8s_4 \\
 & + a_9d_4 + a_{10}V_P. \quad (3)
 \end{aligned}$$

The DZ33 model includes 28 monopole terms and five macroscopic terms discussed in the DZ10 model above with one

extra pairing term. Although the DZ10 and the DZ33 are believed to have similar physics and the same shell structure, the DZ10 cannot be understood as a simplified type of the DZ33 model due to the large differences of monopole terms [39]. Detailed discussions on the DZ33 models may be found in Refs [37,39,40] and references therein.

The formulation of the GK relations is that the interactions between nucleon-nucleon ( $n$ - $n$ ,  $n$ - $p$ ,  $p$ - $p$ ) can be canceled to a large extent in first order in considering an extreme single-particle model, serving as a simple probe to the unknown nuclear force to date. A given mass of a nucleus can be determined with an error bar of 150 keV if the five known masses around this nucleus are known, which is even applicable in regions away from the  $\beta$  stability line. In addition, Ref. [41] suggested an idea without action that a possible way to constrain mass models and improve the mass predictions is to combine the binding energies and the GKs together to be optimized via such the weighted sum method discussed before. Finally, the specific implementation is achieved in this paper in an easier and more rigorous way. There are two commonly used GKs:

$$\begin{aligned} \Delta M_{\text{GK}} = & M(N+2, Z-2) - M(N, Z) + M(N, Z-1) \\ & - M(N+1, Z-2) + M(N+1, Z) \\ & - M(N+2, Z-1) \end{aligned} \quad (4)$$

and

$$\begin{aligned} \Delta M_{\text{GK}} = & M(N+2, Z) - M(N, Z-2) + M(N+1, Z-2) \\ & - M(N+2, Z-1) + M(N, Z-1) - M(N+1, Z), \end{aligned} \quad (5)$$

where  $M$ ,  $N$ ,  $Z$  denote the nuclear mass, neutron number, proton number, respectively.

### III. RESULTS AND DISCUSSIONS

The objective function is defined as the root mean square deviations between predicted and measured values. Our experimental data are expanded with the  $\alpha$  decay energies and the GKs. The binding energies can be easily obtained and the following two observables are indirectly extracted from mass differences. The  $Q_\alpha$  values can be obtained by a relationship of mass differences between a parent nucleus and its daughter, namely,  $Q_\alpha = -\text{BE}(Z, N) + \text{BE}(Z-2, N-2) + \text{BE}_\alpha$ , where  $\text{BE}_\alpha$  is the binding energy for  $^4\text{He}$  nuclei. As for the target of GKs, we define that a set of GKs can give a value called  $\Delta M_{\text{GK}}$  shown in Eq. (4), and the differences between the theoretical  $\Delta M_{\text{GK}}^{\text{theo}}$  and the experimental  $\Delta M_{\text{GK}}^{\text{exp}}$  can be obtained to be minimized. Equation (4) is chosen to perform such a calculation. In addition, one may argue that the objectives of BE and  $Q_\alpha$  may have the priority higher than GKs in optimization since the relative scale of GKs is smaller than other two objectives, resulting in that the obtained result is too unstable to adopt. In general, one of the most effective ways to handle this issue is to normalize objective functions so that they become dimensionless. Actually, the normalization procedure is already implemented in NSGA-III. There may be other paths to tackle such a problem besides the normalization procedure, which deserves further investigations. The

optimization of these three targets is characterized by the following:

$$\begin{aligned} f_1 &= \sigma_{\text{BE}}, \\ f_2 &= \sigma_{Q_\alpha}, \\ f_3 &= \sigma_{\Delta M_{\text{GK}}}, \\ \sigma_A &= \sqrt{\frac{\sum_{i=1}^N (A^{\text{exp}} - A^{\text{theo}})^2}{N}}. \end{aligned} \quad (6)$$

Shown in Fig. 3 are the Pareto fronts by using the MOO approach for the three mass models. Those unreasonable solutions with  $\sigma_{\text{BE}}$  above 5 MeV were previously removed out from the PF results. The first point to note from Fig. 3 is that the best accuracy solution of each objective is found, which tells us the accuracy limit of models for different physical observables, helping theorists to search for missing ingredients. Second, besides the accuracy of binding energies, the accuracy of the byproducts also can represent the reliability and the capacity of models. The improvement of the two observables is significant with a little sacrifice on the accuracy of binding energies. One can see that the high level of accuracy of masses to a large extent is at the price of other two observables, in particular for the BW2 and the DZ10. Taking the BW2 as an example, we calculate the deviations of objective function values between the mass optimal and its nearest suboptimal solution, namely,  $\Delta(f_1, f_2, f_3) = (-0.03, 0.095, 0.002)$  MeV. In fact, the change of 0.01 MeV for  $\alpha$  decay energies can affect the precision of  $\alpha$  decay half-life at at least an order of magnitude. Globally speaking, the  $\sigma_{Q_\alpha}$  values can be considerably improved from about 1.2 to 0.95, 0.4 to 0.3, and 0.35 to 0.2 MeV for the BW2, the DZ10, and the DZ33, respectively. The DZ models describe the consistency of GKs better than the BW2, partly due to more physics considered, partly because the DZ models have the shell-model assumptions, and thus are inherently compatible with GKs [41].

In situations of so many choices, hundreds or even thousands of nondominated solutions, in general, one feels puzzled when following the idea that each solution is considered equally good from the aspect of MOO. It is of great interest to identify the potential solutions from PF in terms of prediction performance. Predictions of neutron-rich nuclei have been a longstanding challenge for researchers since their structure is drastically changed compared to stable nuclei. Moreover, the disagreement between models is most serious in the neutron-rich region. With advances in the field of experimental facilities, an increasing number of neutron-rich nuclei are being produced in the laboratory. With new mass data in hand, it gives us an opportunity to judge the predictive power of models and help us ultimately to select more predictive solutions from the PF compared to the mass optimal solutions. The neutron-rich nuclei chosen to be tested are mostly not included in the fitting set. The DZ10 and the DZ33 are employed for this test.

First, the whole nuclear mass data are divided into two parts, the fitting set from the AME20 and the validation set consisting of neutron-rich nuclei from very recent measurements [43–46]. Second, the model with the mass optimal solution is used to calculate the RMSD with respect to the

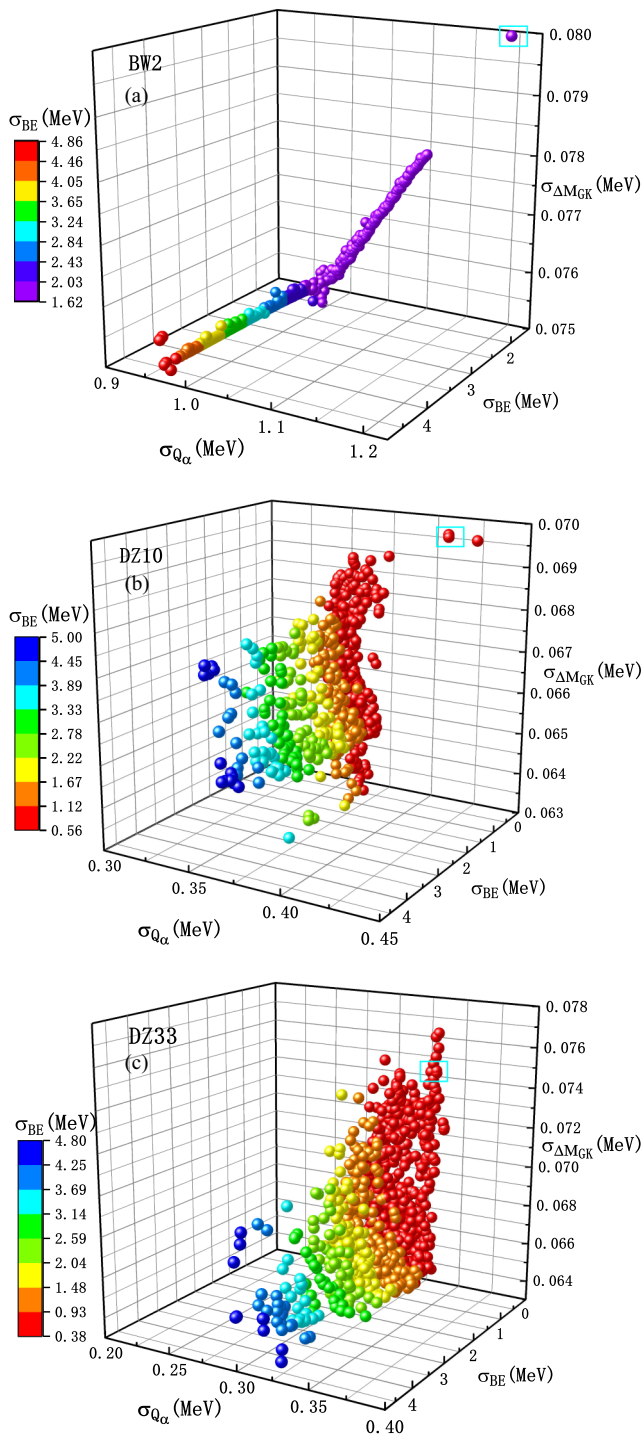


FIG. 3. Every globule represents a nondominated solution, and its color denotes the accuracy of masses to guide eyes. The solutions surrounded by indigo boxes are the mass optimal solutions. The measured binding energies for nuclei with  $N, Z \geq 8$  as well as uncertainties smaller than 100 keV, and  $\alpha$  decay energies limited in even-even nuclei are taken from the latest AME20 [42].

validation set as a benchmark. Finally, the potential solutions from PF may be found if their corresponding accuracy is better than the value calculated by the mass optimal. There are over 50 potential solutions to be picked after this process for

both models, and we define the set of these potential solutions as the potential set (PS). It should be emphasized that the distributions of  $\sigma_{BE}$  values in Fig. 3 range from a few hundreds of keV all the way down to very large 5 MeV, but only a few solutions can achieve better accuracy than the mass optimal solution. Meaningful insights into the PS may be gained by performing statistical analysis on it.

Table I presents an overview of the performance of the PSs on the validation set and the fitting set from partial and global perspectives. In Table I, with the vertical bar in table, the analysis is divided into two parts according to different mass data sets chosen, namely, the validation set and the fitting set. The second column represents the RMSD with respect to the validation set by using the models with the mass optimal solutions. For comparison, the third column refers to the smallest RMSD by using the best solutions from PS. One can see that the accuracy of masses for the validation set are considerably reduced by 50 and 32 percent for DZ10 and DZ33, respectively, by using the best solutions in the PSs compared to the mass optimal. From the fourth column to the last one, every term is described as mean value  $\pm$  standard deviation for describing the central position and the varying scale within observables. The fourth column corresponds to the statistical description of binding energies. The last three columns refer to the statistical description of three objective values, and they provide us, in some sense, with the original accuracy of the models without the mask of overfitting. These actual objective values of PSs near-perfectly match the balance condition discussed before. The values of  $\sigma'_{Q\alpha} = 0.367 \pm 0.019$  and  $\sigma'_{\Delta MGK} = 0.066 \pm 0.001$  MeV are almost located in the middle of each axis for DZ10, namely, the perfect balance between “the best” and “the worst”. The DZ33 also displays a similar trend. It seems that  $\sigma'_{BE} = 0.766 \pm 0.08$  and  $\sigma'_{BE} = 0.502 \pm 0.033$  MeV may provide the valuable anchors on the realistic accuracy of masses for the DZ10 and the DZ33, respectively. Another important advantage of MOO is that our results are tied with statistical uncertainty which comes from various solutions, and the statistical uncertainty of parameters for the DZ10 model is shown in Table II.

In recent years, Orford *et al.* [44] suggested that the DZ model is unsatisfactory in reproducing the mass values of neutron-rich nuclei, namely, Nd and Sm isotopes. To justify this claim, we then compare the mass values obtained by using the DZ10 (with PS) with the measurements of Nd and Sm. As shown in Fig. 4, the theoretical results of  $^{160}\text{Nd}$  and  $^{164}\text{Sm}$  are in good agreement with experimental results. As for other neutron rich isotopes of Nd and Sm, the present differences between theoretical and experimental values are relatively large, which is in accordance with Ref. [44]. It is expected that more mass models will be equipped with MOO strategies to further explore the neutron rich regions.

In the context of reliable extrapolations, now the two models with the potential sets can be used to predict masses across the whole nuclear chart. As mentioned before, although existing mass models give little deviations for available nuclei, it becomes a totally different story when it comes to extrapolations. It will be interesting to see whether the extrapolations still remain stable when the models employ the solutions in the PSs, and whether the theoretical spread between DZ10

TABLE I. Detailed results (scale in MeV) of the potential sets of the models on the validation set and the fitting set (divided by the vertical line).

model	$\sigma_{\text{BE}}^{\text{opt}}$	$\sigma_{\text{BE}}^{\text{PS}}$	$\sigma_{\text{BE}}^{\text{PS}'}$	$\sigma'_{\text{BE}}$	$\sigma'_{Q_\alpha}$	$\sigma'_{\Delta M_{\text{GK}}}$
DZ10	0.405	0.204	$0.337 \pm 0.046$	$0.766 \pm 0.08$	$0.367 \pm 0.019$	$0.066 \pm 0.001$
DZ33	0.135	0.091	$0.12 \pm 0.019$	$0.502 \pm 0.033$	$0.314 \pm 0.015$	$0.07 \pm 0.002$

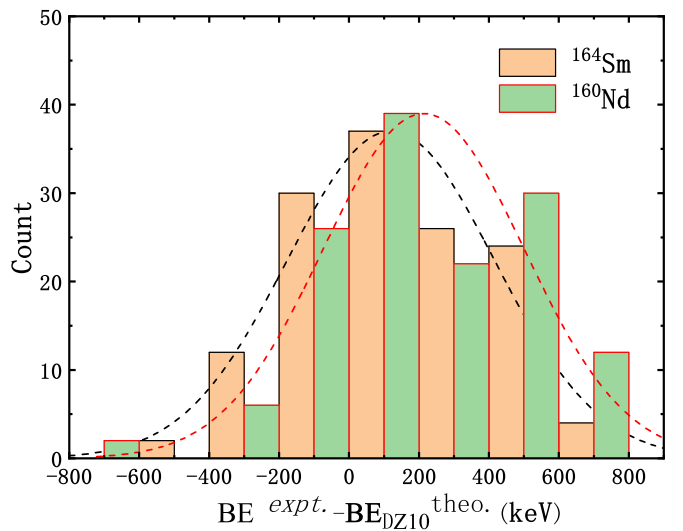
and DZ33 can be systematically reduced. This leads to the following comparisons. Figure 5 shows two evaluations of the extrapolation differences for the models, one is the differences for the model itself and the other is the differences between models. We start by evaluating extrapolation differences for the model itself. First, we can get corresponding nuclear mass tables by using the model with these potential solutions, in which the predictions between two drip lines are limited in even-even nuclei for avoiding the odd-even effects and reducing computational cost. Second, to systematically estimate the uncertainties of models in a credible way, each mass table should be compared to the rest of the mass tables. Quantitatively, each mass table is an individually selected one at a time to calculate the standard deviations with all the remaining mass tables in pairs. Third, these obtained standard deviations with respect to one mass table are further calculated as average values denoted as  $\sigma_{\text{ave}}^{\text{BE}}$ . For instance, assuming that the number of the mass table is 100, each mass table then corresponds to 99 standard values, and the average value of these 99 standard deviations relative to one mass table is obtained. The distributions of all average values are shown in panel (a) of Fig. 5. In this way, it may be insightful to give the robustness of theoretical predictions and estimate theoretical uncertainties. From Fig. 5, one can easily see that the distributions of uncertainties are mostly concentrated on the order of about 0.6 MeV in the DZ33 model, which fairly agrees the accuracy that most models reach, while the range of the uncertainties in the DZ10 model are relatively large from 1 to 2 MeV. This suggests that the predictions by the DZ33 within the PSs may be more stable and reliable than the results of the DZ10 model.

TABLE II. Based on the results of PSs, each parameter shown in the second column is calculated as mean value  $\pm$  standard deviation to describe the statistical uncertainty (in MeV) for the DZ10 formula. For the purpose of comparison, we also provide the parameters of the mass optimal solution, named Case I.

Quantity	Present	Case I
$a_1$	$0.707 \pm 0.001$	0.705
$a_2$	$17.789 \pm 0.03$	17.747
$a_3$	$16.399 \pm 0.114$	16.251
$a_4$	$6.566 \pm 0.599$	6.102
$a_5$	$37.343 \pm 0.107$	37.356
$a_6$	$52.476 \pm 0.495$	52.661
$a_7$	$0.448 \pm 0.015$	0.463
$a_8$	$2.091 \pm 0.075$	2.104
$a_9$	$0.023 \pm 0.0008$	0.021
$a_{10}$	$39.789 \pm 1.246$	41.48

A logical next step is to apply the above comparative method for assessing extrapolation differences between the DZ10 and the DZ33. Analogously, supposing that both models have 100 mass tables, choosing the first mass table from the DZ10 calculates the standard deviations in pairs with all the mass tables from the DZ33. Then, these 100 standard deviations are obtained and also taken as the average values named as  $\sigma_{\text{ave}}^{\text{BE}'}$ . The second mass table is selected to do the same calculations until the last one done. The above calculations are performed for the DZ10 and vice versa for the DZ33, and the distributions of results are shown in Fig. 5(b). In Fig. 5(b), it is obvious that the range of extrapolation differences between the models are larger than that from the upper panel. The solutions at the far right of Fig. 5(b) show pretty large uncertainty, resulting in these solutions being unfeasible to adopt predictions and can be eliminated from the PSs thus further reducing the extrapolation differences.

As discussed above, one of the possible reasons, causing the large extrapolation discrepancies between models, is the overfitting phenomenon. In turn, if the discrepancies between models can be reduced, the overfitting problem may be alleviated to some extent. To address this issue, the two mass evaluations, obtained by using the mass optimal solution of the DZ10 and the DZ33, are added in PSs, respectively. The calculated values corresponding to the mass optimal solution are marked by arrows in Fig. 5. It is clear that in Fig. 5(a) the extrapolation differences between the potential set and the mass optimal solution are relatively large for both models.

FIG. 4. Histograms of the BE differences between experimental and theoretical DZ10 values for  $^{160}\text{Nd}$  and  $^{164}\text{Sm}$ . The dotted line represents the main trend of these bars.

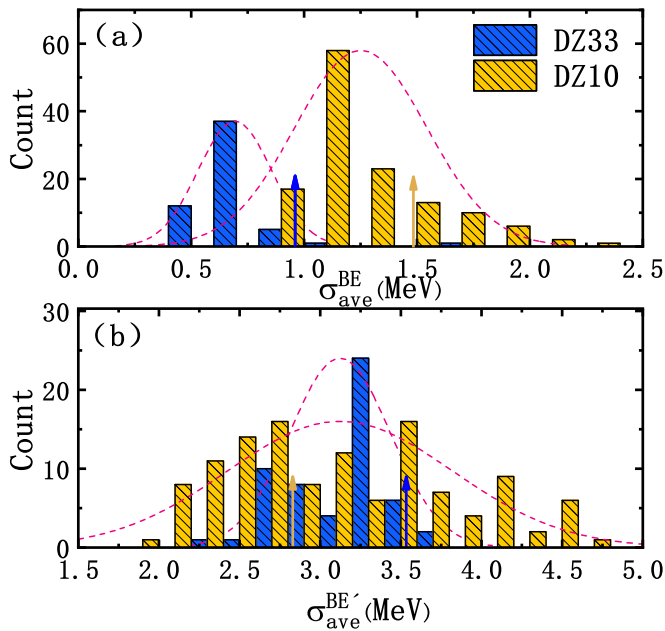


FIG. 5. The extrapolation differences for the model itself are shown in the upper panel and obtained by comparing all the mass evaluations from one model with PS, and the extrapolation differences between DZ10 and DZ33, which is done in a way similar to the above, are shown in the lower one. The dotted red line indicates the main trend of these bars for clarity. The blue (yellow) arrow, respectively, represents the comparison results between the mass optimal solution and the potential set for the DZ33 (DZ10).

This manifests that the extrapolation uncertainties of potential sets are lower than the results of the mass optimal for the models themselves. Last but not least, let us pay attention to extrapolation differences between DZ10 and DZ33. In Fig. 5(b), the blue (yellow) arrow represents the result of mass optimal of DZ33 (DZ10) in comparison with the potential set of DZ10 (DZ33). It is evident that the extrapolation comparison, between the mass optimal of DZ33 and the potential set of DZ10, is large in contrast with the potential set of DZ33. The extrapolation comparison, between the mass optimal of DZ10 and the potential set of DZ33, is similar to the above, albeit indistinctively. This result indicates that the extrapolation discrepancies between DZ10 and DZ33 can be somewhat

reduced. Through these comparisons, one may conclude that, by taking into account these physical constraints with MOO methods, the overfitting problem can be alleviated to some extent.

#### IV. SUMMARY AND OUTLOOK

In conclusion, we have employed the multiobjective optimization to refine the BW2, the DZ10, and the DZ33 by simultaneously including the binding energy, the  $\alpha$  decay energy, and the GKs into fitting procedures. During this process, the accuracy of the  $Q_\alpha$  and the GK values can be noticeably improved for a small price of consistency of the binding energies, suggesting the existence of overfitting problems in current mass formulas. By incorporating these physical features into the fitting space, this not only serves to lower RMSD for those quantities but also improves the extrapolation ability of masses. Comparative study has been carried out for selecting the more potential solutions in the extrapolation issue from the Pareto front in contrast to the overfitted mass optimal solution. We then performed a more thorough and systematic test on the performance of the potential sets. In addition, the statistical uncertainty for the DZ10 model is given due to features of the MOO approach.

The extrapolation differences for the models within the potential sets were also reasonably evaluated, and it was shown that the DZ33 model yields more stable results than the DZ10 model, which is expected to employ the DZ33 for the large distance extrapolations. The potential solutions were further determined via the comparisons between the predictions of models, thus reducing the extrapolation differences obviously. The extrapolation differences between DZ10 and DZ33 were reduced, hinting that the overfitting problem has been somewhat handled. The method for evaluating the extrapolation differences developed in this work can be extended to other mass formulas in the current market, like density functionals or macro-microscopic mass models.

#### ACKNOWLEDGMENT

This work is supported by the National Natural Science Foundation of China (Grants No. 12075121 and No. 11605089), and by the Natural Science Foundation of Jiangsu Province (Grants No. BK20150762 and No. BK20190067).

- [1] D. Lunney, J. Pearson, and C. Thibault, *Rev. Mod. Phys.* **75**, 1021 (2003).
- [2] A. C. Larsen, A. Spyrou, S. N. Liddick, and M. Guttormsen, *Prog. Part. Nucl. Phys.* **107**, 69 (2019).
- [3] T. Yamaguchi, H. Koura, Y. A. Litvinov, and M. Wang, *Prog. Part. Nucl. Phys.* **120**, 103882 (2021).
- [4] J. Erler, N. Birge, M. Kortelainen, W. Nazarewicz, E. Olsen, A. M. Perhac, and M. Stoitsov, *Nature (London)* **486**, 509 (2012).
- [5] Q. Z. Chai, Y. Qiang, and J. C. Pei, *Phys. Rev. C* **105**, 034315 (2022).
- [6] L. Neufcourt, Y. Cao, W. Nazarewicz, F. Viens *et al.*, *Phys. Rev. C* **98**, 034318 (2018).
- [7] G. Garvey, W. Gerace, R. Jaffe, I. Talmi, and I. Kelson, *Rev. Mod. Phys.* **41**, S1 (1969).
- [8] Z. Niu and H. Liang, *Phys. Lett. B* **778**, 48 (2018).
- [9] R. Utama and J. Piekarewicz, *Phys. Rev. C* **96**, 044308 (2017).
- [10] R. Utama and J. Piekarewicz, *Phys. Rev. C* **97**, 014306 (2018).
- [11] Z. M. Niu, J. Y. Fang, and Y. F. Niu, *Phys. Rev. C* **100**, 054311 (2019).
- [12] A. Sharma, A. Gandhi, and A. Kumar, *Phys. Rev. C* **105**, L031306 (2022).
- [13] M. R. Mumpower, T. M. Sprouse, A. E. Lovell, and A. T. Mohan, *Phys. Rev. C* **106**, L021301 (2022).
- [14] A. E. Lovell, A. T. Mohan, T. M. Sprouse, and M. R. Mumpower, *Phys. Rev. C* **106**, 014305 (2022).

- [15] A. Sobiczewski and Y. A. Litvinov, *Phys. Rev. C* **90**, 017302 (2014).
- [16] A. Sobiczewski and Y. A. Litvinov, *Phys. Rev. C* **89**, 024311 (2014).
- [17] A. Pastore, D. Neill, H. Powell, K. Medler, and C. Barton, *Phys. Rev. C* **101**, 035804 (2020).
- [18] S. Goriely, N. Chamel, and J. M. Pearson, *Phys. Rev. C* **82**, 035804 (2010).
- [19] S. Goriely, N. Chamel, and J. M. Pearson, *Phys. Rev. C* **88**, 024308 (2013).
- [20] M. Liu, N. Wang, Y. Deng, and X. Wu, *Phys. Rev. C* **84**, 014333 (2011).
- [21] E. Sahin, M. Doncel, K. Sieja, G. De Angelis, A. Gadea, B. Quintana, A. Gorgen, V. Modamio, D. Mengoni, J. Valiente-Dobon *et al.*, *Phys. Rev. C* **91**, 034302 (2015).
- [22] A. Ozawa, T. Kobayashi, T. Suzuki, K. Yoshida, and I. Tanihata, *Phys. Rev. Lett.* **84**, 5493 (2000).
- [23] M. Rejmund, S. Bhattacharyya, A. Navin, W. Mittag, L. Gaudefroy, M. Gelin, G. Mukherjee, F. Rejmund, P. Roussel-Chomaz, and C. Theisen, *Phys. Rev. C* **76**, 021304(R) (2007).
- [24] M. A. Babyak, *Psychosom Med.* **66**, 411 (2004).
- [25] A. Konak, D. W. Coit, and A. E. Smith, *Reliab. Eng. Syst. Safety* **91**, 992 (2006).
- [26] N. Gunantara, *Cogent Eng.* **5**, 1502242 (2018).
- [27] W. Ye, Y. Qian, and Z. Ren, *Phys. Rev. C* **106**, 024318 (2022).
- [28] C. Igel, N. Hansen, and S. Roth, *Evol. Computation* **15**, 1 (2007).
- [29] E. Zitzler, M. Laumanns, and L. Thiele, TIK Report No. 103, 2001.
- [30] J. D. Knowles and D. W. Corne, *Evol. Comput.* **8**, 149 (2000).
- [31] K. Deb and H. Jain, *IEEE Trans. Evol. Computat.* **18**, 577 (2013).
- [32] K. Deb, A. Pratap, S. Agarwal, and T. Meyarivan, *IEEE Trans. Evol. Computat.* **6**, 182 (2002).
- [33] I. Das and J. E. Dennis, *SIAM J. Optim.* **8**, 631 (1998).
- [34] Y. Yuan, H. Xu, and B. Wang, in *Proceedings of the 2014 Annual Conference on Genetic and Evolutionary Computation* (ACM Press, Vancouver BC Canada, 2014), pp. 661–668.
- [35] M. W. Kirson, *Nucl. Phys. A* **798**, 29 (2008).
- [36] J. Mendoza-Temis, J. G. Hirsch, and A. P. Zuker, *Nucl. Phys. A* **843**, 14 (2010).
- [37] M. W. Kirson, *Nucl. Phys. A* **893**, 27 (2012).
- [38] W. Ye, Y. Qian, and Z. Ren, *Phys. Rev. C* **104**, 064308 (2021).
- [39] C. Qi, *J. Phys. G: Nucl. Part. Phys.* **42**, 045104 (2015).
- [40] J. Duflo and A. P. Zuker, *Phys. Rev. C* **52**, R23 (1995).
- [41] J. Barea, A. Frank, J. G. Hirsch, P. Van Isacker, S. Pittel, and V. Velzquez, *Phys. Rev. C* **77**, 041304(R) (2008).
- [42] M. Wang, W. Huang, F. Kondev, G. Audi, and S. Naimi, *Chin. Phys. C* **45**, 030003 (2021).
- [43] R. Orford, N. Vassh, J. A. Clark, G. C. McLaughlin, M. R. Mumpower, D. Ray, G. Savard, R. Surman, F. Buchinger, D. P. Burdette, M. T. Burkey, D. A. Gorelov, J. W. Klimes, W. S. Porter, K. S. Sharma, A. A. Valverde, L. Varrian, and X. L. Yan, *Phys. Rev. C* **105**, L052802 (2022).
- [44] R. Orford, N. Vassh, J. A. Clark, G. C. McLaughlin, M. R. Mumpower, G. Savard, R. Surman, A. Aprahamian, F. Buchinger, M. T. Burkey, D. A. Gorelov, T. Y. Hirsh, J. W. Klimes, G. E. Morgan, A. Nystrom, and K. S. Sharma, *Phys. Rev. Lett.* **120**, 262702 (2018).
- [45] W. S. Porter, B. Ashrafkhani, J. Bergmann, C. Brown, T. Brunner, J. D. Cardona, D. Curien, I. Dedes, T. Dickel, J. Dudek, E. Dunling, G. Gwinner, Z. Hockenbery, J. D. Holt, C. Hornung, C. Izzo, A. Jacobs, A. Javaji, B. Kootte, K.-G. Koncz, E. M. Lykiardopoulou, T. Miyagi, I. Mukul, T. Murbock, W. R. Plass, M. P. Reiter, J. Ringuette, C. Scheidenberger, R. Silwal, C. Walls, H. L. Wang, Y. Wang, J. Yang, J. Dilling, and A. A. Kwiatkowski, *Phys. Rev. C* **105**, L041301 (2022).
- [46] H. F. Li, S. Naimi, T. M. Sprouse, M. R. Mumpower, Y. Abe, Y. Yamaguchi, D. Nagae, F. Suzaki, M. Wakasugi, H. Arakawa, W. B. Dou, D. Hamakawa, S. Hosoi, Y. Inada, D. Kajiki, T. Kobayashi, M. Sakaue, Y. Yokoda, T. Yamaguchi, R. Kagesawa, D. Kamioka, T. Moriguchi, M. Mukai, A. Ozawa, S. Ota, N. Kitamura, S. Masuoka, S. Michimasa, H. Baba, N. Fukuda, Y. Shimizu, H. Suzuki, H. Takeda, D. S. Ahn, M. Wang, C. Y. Fu, Q. Wang, S. Suzuki, Z. Ge, Y. A. Litvinov, G. Lorusso, P. M. Walker, Z. Podolyak, and T. Uesaka, *Phys. Rev. Lett.* **128**, 152701 (2022).